Journal of Magnetism and Magnetic Materials 499 (2020) 166301

Contents lists available at ScienceDirect

Journal of Magnetism and Magnetic Materials

journal homepage: www.elsevier.com/locate/jmmm

Research articles

Understanding high ordering temperature in Gd_6FeBi_2 magnet: Critical behavior, electronic structure and crystal-field analysis

Guoming Cui[a], Huan Ma[b], Kam Wa Wong[c], Chan Hung Shek[b], Guangcun Shan[d,*], Jiliang Zhang[e,*]

[a] Department of Materials Science and Engineering, Henan Institute of Technology, Xinxiang 453003, China
[b] Department of Materials Science and Engineering, City University of Hong Kong, Kowloon, Hong Kong, China
[c] Department of Physics, City University of Hong Kong, Kowloon, Hong Kong, China
[d] School of Instrument Science and Opto-electronics Engineering & Institute of Quantum Sensing, Beihang University, Beijing 100083, China
[e] Department of Energy & Materials Engineering, Dongguk University-Seoul, Seoul 04620, South Korea

ARTICLE INFO

Keywords:
Rare earth alloys and compounds
Crystal and ligand fields
Electronic band structure
Magnetisation

ABSTRACT

Gd_6FeBi_2 is reported as the only one room-temperature magnet among more than hundreds of compounds with its structural type, which makes it more attractive in potential applications. To reveal the origin of such high ordering temperature, critical behaviors, electronic structure and crystal-field effects of Gd_6FeBi_2 are investigated in this work. The short-range Gd-Fe ferrimagnetic interaction is supported by the crystal and electronic structure analyses. Unlike the strong Fe-Fe exchange interactions, the Gd-Fe exchange interaction shows limited influence on the critical exponents determined by long-range exchange interactions, which seems a common feature in rare earth – transition metal based alloys without exchange interactions between transition-metal atoms. However, the strong Gd-Fe hybridization reduces the influence of vibronic couplings on the short-range exchange interaction and thus allows a high T_c. The broadening or splitting mechanism of Gd 4*f*-electron bands is addressed based on crystal-field analysis and likely another factor for elevated T_c in Gd_6FeBi_2 and Gd-based compounds with non-magnetic elements. Different magnetic behaviors among isostructural compounds, and the relationship between the band splitting and crystal-field effects is also discussed.

1. Introduction

Most heavy rare-earth (*RE*) metals possess very large magnetic moment ideal for many magnetic applications, but the low magnetic ordering temperature inhibits their application in practice. To overcome this drawback, many efforts are made to develop *RE*-based *RE-TM* (*TM*, transition metal) intermetallic compounds, because the strong *RE-TM* or *TM-TM* magnetic interactions can effectively elevate the ordering temperature compared with the indirect 4*f*-4*f* interactions between *RE* atoms, while the small magnetic moment of *TM* will not change the net magnetic moment of these compounds significantly. Another chemical element, generally from the p-block of main groups, is usually added into these *RE-TM* systems to produce even greater diversity of new compounds and structures, as well as to improve properties.

A new family of Fe_2P type with the general formula RE_6TMX_2 (*RE* = Gd-Tm, and Lu; *TM* = Mn, Fe, Co, Ni and Ru; and *X* = Al, Ga, Sn, As, Sb, Bi, S, Se and Te) firstly discovered in 2003 by different research groups independently is a typical example of such strategy [1–5]. These compounds show fruitful magnetic behaviours as characterized by multiple magnetic transitions and the absence of magnetic moment from *TM* in many members [6–8]. Some members also show large magnetocaloric effects around their Curie temperatures (T_c) [9–12]. However, the reported magnetic ordering temperature of all members are lower than room temperature except Gd_6FeBi_2 [11], which has an ordering temperature up to 350 K, higher than that of most Gd-based intermetallic compounds [13].

Due to the great potential for practical applications, many efforts are made to understand the origin of high ordering temperature or strong magnetic interactions in these Gd-based compounds with high T_c, e.g. Gd_5Si_4 (336 K) and Gd_4Bi_3 (340 K) [14,15]. A typical explanation for the compounds with non-magnetic elements (NMEs) is the Ruderman-Kittle-Kasuya-Yosida (RKKY) interaction, where the *f*-shell electron spins couple with those of a neighbouring Gd atom through the conduction electrons. Such indirect exchange interaction can induce the fluctuation of T_c depending on the conduction electrons and distance between neighbouring magnetic atoms, but it is difficult to elevate T_c significantly because of the nature of indirect interactions. Later it is realized that the high T_c can be induced by extra magnetic moment

* Corresponding authors.
E-mail addresses: gcshan@buaa.edu.cn (G. Shan), jiliangz@dongguk.edu (J. Zhang).

https://doi.org/10.1016/j.jmmm.2019.166301
Received 3 October 2019; Accepted 13 December 2019
Available online 14 December 2019
0304-8853/

from the localized/polarized 5*d* electrons in Gd [16], or extra magnetic moment from NMEs (e.g. Bi in Gd_4Bi_3) due to strong interactions or polarizations [17]. Very recently, the low-temperature structure of Gd_6FeBi_2 was determined from single crystals, and the DFT calculations based on the structural model did show the magnetic moment from 5*d* electrons of Gd and a ferrimagnetic interaction between Gd and Fe, accounting for the high ordering temperature in Gd_6FeBi_2 [18]. However, multiple magnetic transitions (and very likely structural transitions) exist in this family and some may induce a significant change of interactions between atoms. Thus, to understand the origin for the high T_c, it is more proper to use the data from the high-temperature magnetic phase for analysis.

In this work, we attempt to reveal the magnetic exchange interactions from the critical behaviours of the high-temperature magnetic phase and understand the chemical and magnetic interactions in the compound from its electronic structure and crystal-field analysis, so that the structural landscape for the enhanced magnetic exchange interactions can be constructed.

2. Experimental

Gd_6FeBi_2 ingots were fabricated by arc melting the mixtures of pure constituent elements Gd (99.9 wt%), Fe (99.95 wt%), and Bi (99.9 wt%) under a Ti-getterred argon atmosphere. A small extra amount of Bi (0.4%, 0.6%, 0.8%, 1.0% and 1.2%, respectively) were added into samples to compensate for the loss of Bi due to vaporization during arc melting. All ingots were remelted for four times to improve compositional homogeneity. After melting, all ingots were sealed into high vacuum quartz tube and then annealed at 1073 K for 10 days. Finally, the sealed quartz tube was quenched into ice water. Phase identification was conducted on a Philips X'pert X-rays diffractometer (Cu Kα, $\lambda = 0.15406$ nm). Isothermal magnetisation were measured using a LakeShore VSM with a maximum field of up to 50 kOe. The applied magnetic fields (H_E) were corrected for the demagnetization to get the internal field $H = H_E\text{-}NM(T,H_E)$, where N is the demagnetion factor and M is the measured magnetization. Demagnetization factors were calculated from low-field magnetization following the method in given in reference [19]. To further reduce the effects of demagnetization, only data obtained from the field above 0.5 T were used for analysis. Experimental electronic structures were measured by X-ray photoelectron spectroscopy (XPS) using an ULVAC-PHI 5802 spectrometer equipped with a monochromatized Al Kα radiation ($h\upsilon = 1486.6$ eV) in vacuum of about 10^{-9} mbar. All samples were sputtered by Ar ion to remove the O_2-contiminated surface before the measurement.

3. Scaling analysis

A variety of physical systems exhibited critical phenomena, in which the physical behaviors can be well described using a set of parameters. And the second order magnetic transition is a well-known critical point. For such magnetic systems, the low-temperature magnetization and high-temperature susceptibility can be well described using a scaling rule constructed by critical exponents. According to the scaling hypothesis, the mathematical definitions of these critical exponents for magnetic systems can be described as follows [20]:

$$M_S(T) = M_0(-\varepsilon)^{\beta}, \varepsilon < 0 \quad (1)$$

$$\chi_0^{-1}(T) = \Gamma\varepsilon^{\gamma}, \varepsilon > 0 \quad (2)$$

$$M = DH^{1/\delta}, \varepsilon = 0 \quad (3)$$

where:

$\varepsilon = (T - T_C)/T_C$, the reduced temperature; M_0, Γ, D, the critical amplitudes;

β, a critical exponent associated with the spontaneous magnetization M_S;

γ, a critical exponent associated with the initial magnetic susceptibility χ_0;

δ, a critical exponent associated with the critical isothermal magnetization at T_c.

These exponents are not independent of each other, but correlated by some relationships. And finally a scaling hypothesis, describing the magnetic equation of state, is achieved. Using the scaling hypothesis the magnetization can be expressed as:

$$M(H, \varepsilon) = |\varepsilon|^{\beta} f_{\pm}\left(\frac{H}{|\varepsilon|^{\beta+\gamma}}\right) \quad (4)$$

where $f_{\pm}$ are regular analytical functions with f_+ for $\varepsilon > 0$, and f_- for $\varepsilon < 0$. In terms of scaled magnetization $m \equiv |\varepsilon|^{-\beta}M(H, \varepsilon)$ and scaled field $h \equiv |\varepsilon|^{-(\beta+\gamma)}H$, the Eq. (4) can be written into the more familiar form:

$$m = f_{\pm}(h) \quad (5)$$

It is clear that the above equation above implies that the scaled m plotted as a function of the scaled h will fall onto two different universal curves described by f_+ and f_- respectively, for true scaling relations and right choice of these critical exponents.

Although the exponents generally show universal properties in the asymptotic region ($\varepsilon \to 0$), various systemic trends or crossover phenomenon are often observed, mostly due to the presence of various competing couplings and/or disorder. In the present case, Gd_6FeBi_2 shows non-Curie-Weise paramagnetic behaviors, in contrast to the HCP Gd with clearly Cuie-Weise paramagnetic behaviors above magnetic transition [21]. Therefore it is useful to introduce the temperature-dependent effective exponents for $\varepsilon \neq 0$, which are defined as [20]:

$$\beta_{eff}(\varepsilon) = \frac{d[ln M_S(\varepsilon)]}{d(ln\varepsilon)} \quad (6)$$

$$\gamma_{eff}(\varepsilon) = \frac{d[ln\chi_0^{-1}(\varepsilon)]}{d(ln\varepsilon)} \quad (7)$$

These effective exponents are general non-universal, but approach universal exponents in the asymptotic limit.

4. Results and discussion

Among the synthesized samples, the one with an extra 0.8% Bi has the best phase purity. The XRD pattern of Gd_6FeBi_2 at room temperature is similar to the simulated XRD pattern generated from structure parameters obtained by single crystals despite the slight shift due to different temperatures (see Fig. 1) [18]. All reflections in XRD pattern of Gd_6FeBi_2 can be well indexed according to the Fe_2P-type structure, and gives the unit cell of $a = 8.366(5)$ Å and $c = 4.243(4)$ Å, in good agreement with previous reports [5,11]. RKKY indirect exchange interaction, which is common in *RE*-based compounds without other NMEs, can induce the fluctuation of T_c depending on the concentration of conduction electrons and distance between neighbouring magnetic atoms. Our recent work shows that exchange interaction in Gd_6CoTe_2 is dominated by the RKKY mechanism, while extra short-range exchange interactions exist in Gd_6FeBi_2 accounting for the high T_c [18]. To understand these exchange interactions, critical behaviors around the T_c are to be first investigated.

4.1. Critical behaviors

Near the transition, the Landau theory of second-order phase transition suggests that the free energy G of a magnetic system can be expanded in the powers of its order parameter M in the following form [22]:

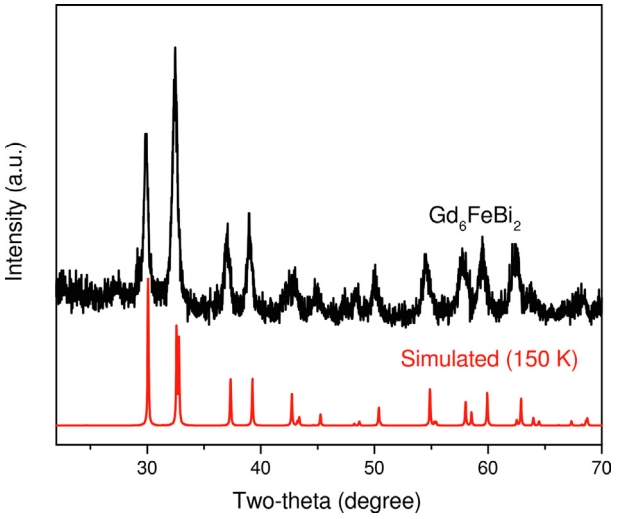

Fig. 1. Experimental XRD patterns (black) of Gd_6FeBi_2 and the simulated pattern (red) from the crystal structure determined at 150 K. (For interpretation of the references to colour in this figure legend, the reader is referred to the web version of this article.)

$$G(T, M) = G_0 + \frac{1}{2}\mathrm{A(T)M^2} + \frac{1}{4}\mathrm{B}(T)M^4 + \cdots\cdots - \mathrm{MH} \tag{8}$$

where coefficients A and B are temperature-dependent parameters, and the last term describes the energy of spins in an external field H. Generally the higher order items can be neglected in practice due to their small values. In the case of equilibrium, the energy is minimized $\left(\frac{\partial G}{\partial M} = 0\right)$, which leads to the magnetic equation of states in the form of Arrott formula [23]:

$$\frac{\mathrm{M}}{\mathrm{H}} = \mathrm{A} + \mathrm{BM^2} \tag{9}$$

Therefore the M^2 versus H/M curves should be straight lines, of which the intercept on the H/M axis determines the ordering transition. As shown in Fig. 2a, the Arrott plots of Gd_6FeBi_2exhibit positive slope, which indicates that the magnetic transition is second-order according to the criterion suggested by Banerjee [24]. It is also noted in Fig. 2a that the plots of Gd_6FeBi_2 show slightly downward from the linearity, because the Arrott plot is actually based on the mean-field approach without considering microscopic exchange interactions and fluctuations in magnetic systems.

Compared with the mean-field theory, both Ising and Heisenberg models include the exchange interaction between spins (short-range/direct interactions). And both models can also give critical exponents for the well-known modified Arrott (MA) relation which can be expressed as [25]:

$$\left(\frac{\mathrm{M}}{\mathrm{H}}\right)^{1/\gamma} = \mathrm{A}\varepsilon + \mathrm{BM}^{1/\beta} \tag{10}$$

Based on the critical exponents β and γ predicted by 3D-Ising and 3D-Heisenberg models (see Table 1) [26], MA plots of Gd_6FeBi_2 are drawn in Fig. 2b and 2c respectively, and all plots seem curved upward from the linearity.

According to Eq. (10), linear extrapolation of the high field portions of the isotherms will give an intercept on both $M^{1/\beta}$ and $\left(\frac{M}{H}\right)^{1/\gamma}$ axis, from which the spontaneous magnetization M_S and the inverse initial susceptibility χ_0^{-1} can be calculated. Using these calculated data, new critical exponents can also be obtained based on Eqs. (1) and (2). The best values of β and γ obtained by fitting Eq. (10) should be self-consistent with the values yielded by fitting Eqs. (1) and (2) to the extrapolated data. To get the best values, we programmed according to the idea which was also introduced in literature [27], and then got the best values fitting our data. Previous work shows that effective exponents converge approaching to the universal exponents only when $\varepsilon < 0.1$ [26]. Thus our estimations on critical exponents were performed using data in the range. After several cycles, the exponents converged into stable values. The values obtained after 30 cycles are $\beta = 0.441(8)$, $\gamma = 1.098(12)$ for Gd_6FeBi_2. Evidently, the MA plot of Gd_6FeBi_2 exhibit good linearity around T_c as shown in Fig. 2d. The spontaneous magnetization M_S and the inverse initial susceptibility χ_0^{-1} obtained using these exponents are then plotted as a function of temperature in Fig. 3a. The fitting of these values to Eq. (1) gives $\beta = 0.439(6)$, $T_c = 347.9(1)$ K, and to Eq. (2) gives $\gamma = 1.107(10)$, $T_c = 348.1(1)$ K. These values are also listed in Table 1. It is distinct that these values are closer to those given by mean-field model rather than 3D-Ising or 3D-Heisenberg model.

Using determined M_S and χ_0^{-1} by the above method (see Fig. 3a), the critical exponents and T_c of high precision can be obtained by following the Kouvel-Fisher (KF) method [28], which is described by an alternative form of Eqs. (1) and (2):

$$\mathrm{M}_S\left(\frac{d\mathrm{M}_S}{dT}\right)^{-1} = (T - T_C)/\beta \tag{11}$$

$$\chi_0^{-1}\left(\frac{d\chi_0^{-1}}{dT}\right)^{-1} = (T - T_C)/\gamma \tag{12}$$

According to the method, in critical regions, the plots of $\mathrm{M}_S\left(\frac{d\mathrm{M}_S}{dT}\right)^{-1}$ vs. T and $\chi_0^{-1}\left(\frac{d\chi_0^{-1}}{dT}\right)^{-1}$ vs. T yield straight lines with slopes $1/\beta$ and $1/\gamma$ respectively, and intercepts of such fitted straight lines on their T axis equal to T_c. The most important advantages of the KF method is: no previous knowledge of Tc is required, and it provides a consistency condition for T_c, namely, the fitting of both plots should give the same value of T_c. The KF plots of Gd_6FeBi_2 is shown in Fig. 3b, and estimated critical exponents and T_C by fitting these straight lines are: $\beta = 0.446(6)$, $T_c = 348.2(1)$ K and $\gamma = 1.092(10)$, $T_c = 348.0(1)$ K.

All these critical exponents estimated from above methods, together with predicted theoretically values from different models, are listed in Table 1. It is evident that values of critical exponents and T_c calculated using both methods match reasonably well, which indicates that these estimated values are self-consistence. However, it is also clear that these values do not match the conventional universality classes. Thus it is necessary to verify whether these critical exponents can produce the scaling equation of state. Taking the values of critical exponents and T_c listed in Table 1, the plots of scaled m against scaled h are drawn in Fig. 4a. These plots depict the two different universal curves distinctly as predicted by the scaling equation Eq. (5), which indicates the reliability of the calculated critical exponents and T_c. The inset of Fig. 4a shows the same plot on log–log scale, which suggests the converging of two curves towards to T_c.

A more rigorous way to confirm whether the estimated values of critical exponents and T_c are reliable and whether the isotherms taken in the critical region obey the scaling equation of state, is to analyze the experimental data in terms of the well-established asymptotic form of the scaling equation given by [29]

$$\frac{\mathrm{h}}{\mathrm{m}} = \pm a_{\pm} + b_{\pm}\mathrm{m^2} \tag{13}$$

where plus and minus signs have the same meaning as that in Eq. (4), a and b are two scaling parameters for Gibbs potential concerning both thermal and magnetic field effects. Then the coefficients in the equation can be related to the critical amplitudes in Eqs. (1) and (2) as

$$(a_-/b_-)^{1/2} = \mathrm{M} = \mathrm{m}_0 \tag{14}$$

$$a_+ = \Gamma = \mathrm{h}_0/\mathrm{m}_0 \tag{15}$$

It is significant that these critical amplitudes m_0 and h_0/m_0 can be obtained by intercepting the universal curves with m^2 and $\frac{h}{m}$ axis in the

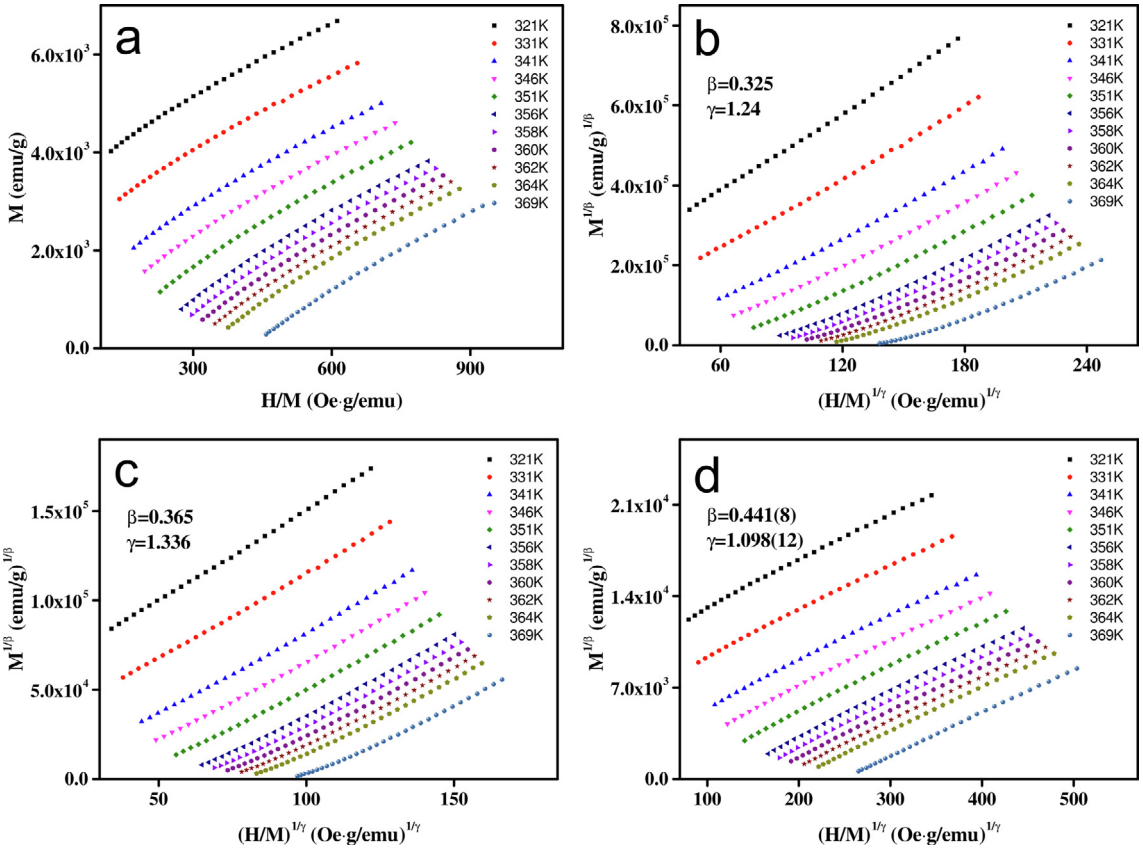

Fig. 2. Arrott plots (a) and modified arrott plots using different exponents: (b) 3D Ising model, (c) 3D Heisenberg model and (d) β = 0.441(8), γ = 1.098(12).

Table 1
Comparison of critical exponents of Gd_6FeBi_2 and different theoretical models.

Composition	Technique	β	γ	Ref.
Gd_6FeBi_2	Modified Arrott Plot	0.441(8)	1.098(12)	Present
	Kouvel-Fisher method	0.446(6)	1.092(10)	Present
3D Ising		0.325	1.241	[26]
3D Heisenberg		0.365	1.386	[26]
Mean Field		0.5	1	[23]

plots of m^2 vs.$\frac{h}{m}$ respectively, as shown in Fig. 4b. These values are determined as: m_0 = 169(6) emu/g, and the effective exchange interaction field h_0 = 11.6(2) kOe.

4.2. Magnetic exchange interaction and electronic structure

In *RE*-based compounds with NMEs, the RRKY interaction is generally the dominant long-range interaction, but other long-range forces like dipolar interaction can also influence the critical fluctuations of magnetization. According to the criterion given by Tadaoff et al [30], such long-range forces can be neglected in case

$$|\varepsilon| \gg [\mu M_S(0)/k_B T_C]^{1/\beta(\delta-1)} \equiv t \quad (16)$$

where $\mu = g\mu_B S$ is the moment of per spin, k_B is Boltzmann constant, and the saturation magnetization $M_S(0)$ can be calculated form Eq. (1) as 1600 Oe. Then using Eq. (16) t is estimated as 2.5 × 10^{-3}, much smaller than the range of |ε|. Thus the dipolar interactions, if present, have a negligible effect on the critical fluctuation of magnetization.

Above analyses on critical behaviors indicate the dominant long-range exchange interactions, while both the deviation from Curie-Weiss paramagnetic behavior above T_c in a linear compound and previous DFT calculation suggest the important role of short-range exchange interaction in Gd_6FeBi_2 for high T_c. Actually the T_c of Gd_6FeBi_2 is much higher than that of its analogue Gd_6CoTe_2 (350 K against 220 K) [31], which is not expected by RKKY interactions.

It is also known that the ferromagnetism/ferrimagnetism-paramagnetism transition is actually the destabilization of magnetic orders by thermal coupling. The scaling equation of state actually involves the role of thermal energy. Since h_0 is the effective exchange interaction field, the product of h_0 and an average effective elementary moment (μ_{eff}) involved in the FM-PM transition, namely the effective exchange energy $\mu_{eff} h_0$, is expected to equal the thermal energy at $T = T_C$. In mean-field model, $\mu_{eff} h_o/k_B T_C$ equal 1.73. Using the value, μ_{eff} is estimated as 4.55μ_B (~6.8μ_B per Gd atom) for the Gd_6FeBi_2 compound, smaller than the theoretical value (7 μ_B per Gd atom) and suggestive of the Gd-Fe ferrimagnetic exchange interaction.

To address the inconsistence between critical exponents and short-range exchange interaction, it is necessary to analyse the structural origin of the Gd-Fe exchange interaction first. Like other RE_6FeBi_2, Gd_6FeBi also presents multiple magnetic transitions, and no evident structural change is observed at low temperature (see Fig. 1). Neutron diffraction experiments show that these transitions are related to non-linear magnetic structures. Unlike other *RE*, Gd is a linear alloy and does not show orbital-spin couplings for conical or helical magnetic structures, and thus the multiple magnetic transitions in are very likely to be related with the crystal-field effects. The typical energy between the ground state and the first excited crystal field state in *RE*s varies from 1 to 10 meV (10 K to 100 K) with the overall spread of all levels up to 20 meV, a value compared to the exchange energy for Gd (25 meV) [32].

Because the magnetic structures of Ho_6FeBi_2 determined by neutron diffraction show no magnetic contribution from Fe [6], different structural features for the Gd-Fe ferrimagnetic interaction are expected in Gd_6FeBi_2. The electronic configure of Fe is $[Ar]3d^64s^2$, which allows a minimum-energy state with paired d electrons corresponding to a nonmagnetic state. However, the spatial extent of 3*d* electron wave

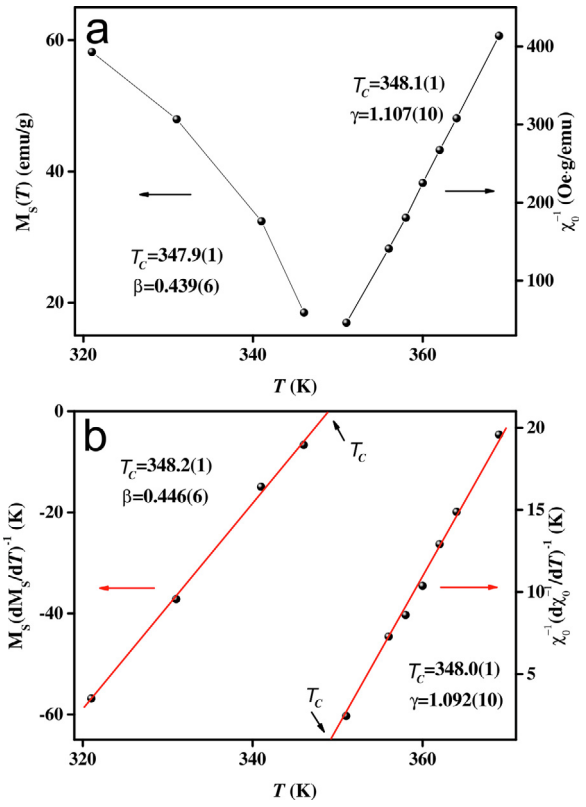

Fig. 3. (a) Temperature variation in spontanous magnetization $M_S(T)$ (left axis) and inverse initial susceptibility $\chi_0^{-1}(T)$ (right axis); (b) Kouvel-Fisher plot of spontanous magnetization $M_S(T)$ (left axis) and inverse initial susceptibility $\chi_0^{-1}(T)$ (right axis). Black solid lines in (a) are guides for eyes, and red straight lines in (b) are due to linear fitting of data. (For interpretation of the references to colour in this figure legend, the reader is referred to the web version of this article.)

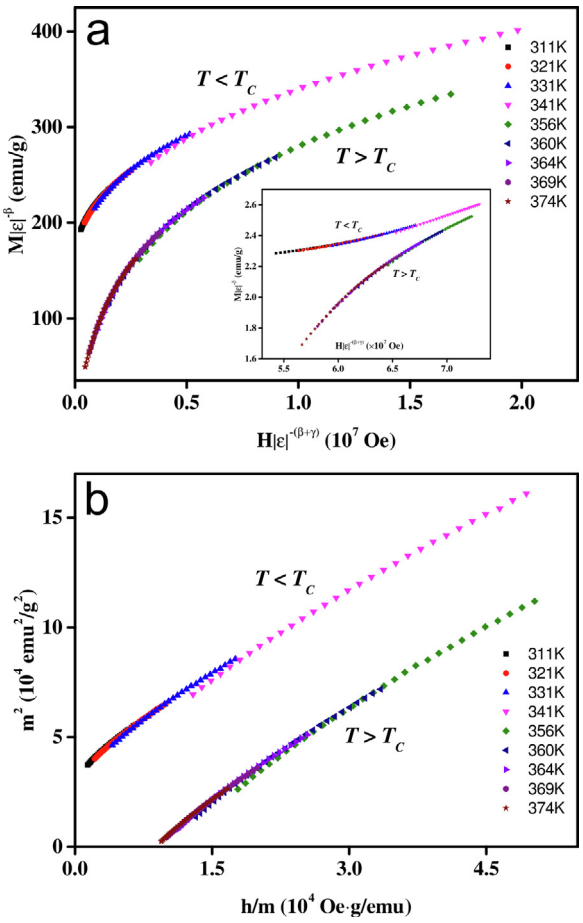

Fig. 4. (a) Scaled magnetization of the Gd_6FeBi_2 compound below and above T_C, using critical exponents given by the Kouvel-Fisher plot. (b) The scaled magnetization and field are plotted in the form of m^2 vs. h/m for the Gd_6FeBi_2 compound. The inset in (a) shows the same plot on a log–log scale.

function is considerably large, and thus 3*d* electron wave functions of neighbouring atoms show a strong overlap, leading to 3*d* electron bands, where the relatively strong effective Coulomb repulsion between 3d electrons can favor situations in which the number of spin up and spin down electrons is no longer equal and leads to the formation of a magnetic moment. In the RE_6TMX_2 family, *TM* atoms are surrounded only by *RE* atoms (Fig. 5a). The absence of *TM-TM* contacts and the low electronic density of states of *s* electron bands in *REs* account for the nonmagnetic state of *TM* in these compounds except Gd analogues. In Gd analogues, the 5*d* electron band of Gd may have an overlap with 3*d* electron bands in *TM*, depending on the Gd-*TM* bond strength. In Gd_6CoTe_2, for instance, the Gd-Co interaction seems similar in strength to other *RE*-Co as characterized by the nearly linear relationship between a/c and atomic radii of *RE* elements (Fig. 5b), because lattice constant a is related to the Fe site and a/c is an indicator of the *RE*-Fe bond strength. In contrast, Gd-Fe interaction is much stronger than other *RE*-Fe interactions in RE_6FeBi_2, which is characterized by the a/c of Gd_6FeBi_2 much smaller than the extrapolated value from the linear relationship between a/c and atomic radii of *RE* elements in other RE_6FeBi_2. Thus a stronger overlap of electron wave functions between Gd 5*d* electron bands and Fe 3*d* electron bands is expected, accounting for the magnetic moment from Fe in Gd_6FeBi_2. Such strong Gd-Fe interaction also benefits the spin polarization of Gd 5*d* electrons for an extra magnetic moment, in consistent with DFT calculations. In Gd_6CoTe_2, however, the overlap should be very weak or negligible due to the weak Gd-Co interaction, and a net magnetic moment from Co may not be expected.

The interactions between Gd and Fe in Gd_6FeBi_2 can be inspected more directly from its electronic structure, as seen in the XPS spectra in Fig. 6. Compared with sharp peaks in their electronic density of states (DOS) around the fermi level E_F in Gd and Fe metals, Gd_6FeBi_2 has a more flat DOS up to several eV below E_F (Fig. 6a), suggestive of Gd-Fe hybridization and in agreement with previous DFT calculations. The low and flat DOS at E_F supports the high stability of Gd_6FeBi_2, because the orbital splitting due to the hybridization allows more low-energy bands. However, the DOS of Gd_6FeBi_2 at E_F is still much larger than that of Gd_4Bi_3 [14], a compound with a high T_c (340 K) due to an extra Bi magnetic moment induced by the strong Gd-Bi hybridization [17]. Thus the magnetic contributions from Gd 5*d* and Fe 3*d* are expected in Gd_6FeBi_2, despite the reduced magnetic moment from *d* electrons due to some unpaired *d* electrons in these elements moved into lower energy orbitals to pair other electrons after the hybridization.

Compared with the strong overlap of *d* electron wave functions between neighbouring atoms in Gd and Fe metals, the overlap is effectively reduced in Gd_6FeBi_2 due to the hybridization and low DOS around E_F. Therefore the exchange interaction between Gd 5*d* and Fe 3*d* Gd_6FeBi_2 in should be weaker than those of Gd 5*d* –Gd 5*d* in Gd and *TM* 3*d* – *TM* 3*d* in Fe, which accounting for critical exponents more close to the values predicted by the long range interactions. In other words, the critical exponents corresponding to the Ising or Heisenbergy model in *Gd-TM* alloys should result from the *TM-TM* exchange interaction, because the Gd-*TM* exchange interaction is not strong enough. Thus the critical behavior of *Gd-TM* alloys can be tuned from the Ising/Heisenbergy model to the mean-field model by hybridizing *TM* with a third element (e.g. metalloid elements). This is exactly the case of Gd_4Co_3 alloys doped by Si: from $\beta = 0.389$ and $\gamma = 1.229$ in Gd_4Co_3 to

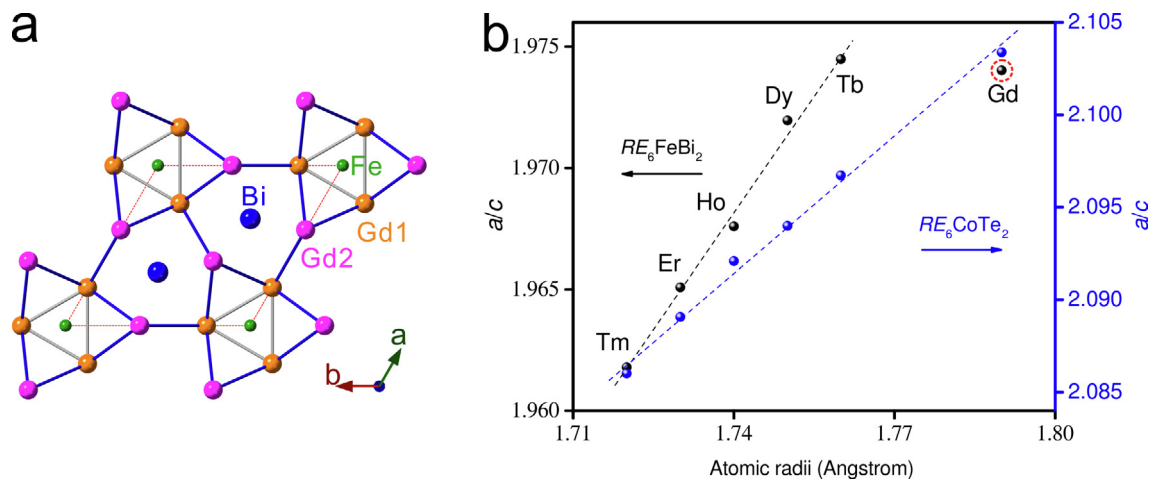

Fig. 5. (a) The representative crystal structure of Gd_6FeBi_2 viewed along c axis, and (b) plots of a/c against atomic radii of *RE* elements in RE_6FeBi_2 (black) and RE_6CoTe_2 (blue). The dashed circle in (b) emphasizes the contraction in the basal plane of Gd_6FeBi_2. (For interpretation of the references to colour in this figure legend, the reader is referred to the web version of this article.)

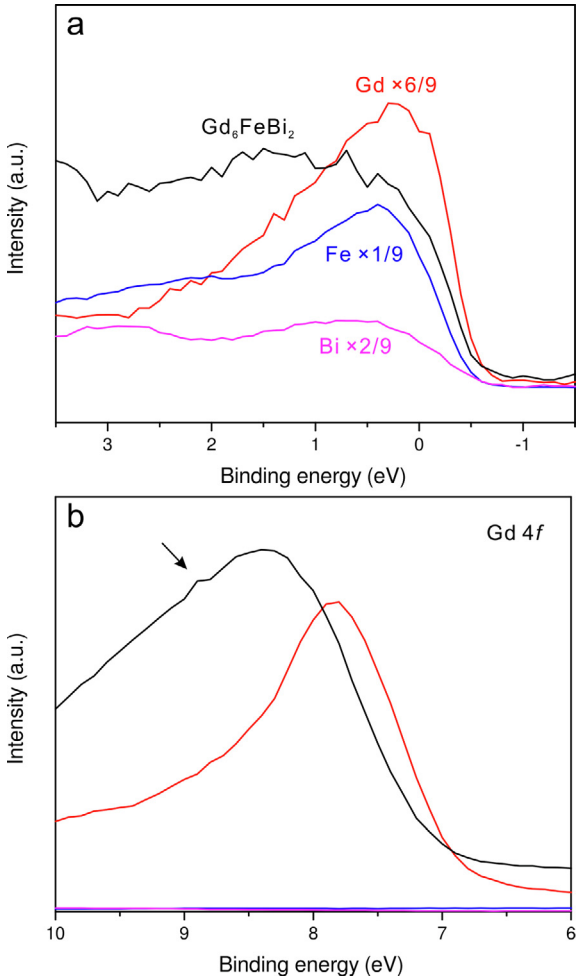

Fig. 6. XPS spectra of Gd_6FeBi_2 and the constitute elements in the valence band (a) and Gd 4*f* region (b). The intensity in XPS spectra of constitute elements is multiplied by their fraction in the formula. In the 4*f* band of Gd_6FeBi_2, a shoulder peak is arrowed and the much high intensity is due to the strong inelastic electronic scattering.

$\beta = 0.465$ and $\gamma = 1.134$ in $(Gd_4Co_3)_{0.9}Si_{0.1}$ [33].

The ordering temperature in these compounds should be related to not only the magnetic moment, but also the vibronic coupling effects. Due to the strong Gd-Fe hybridization, the influence of such coupling on *d* electrons in Gd_6FeBi_2 should be much smaller than those of the Gd metal, and thus the short-range exchange interaction in Gd_6FeBi_2 diminishes more slowly with increased temperatures, accounting for the elevated T_c and the deviation from the Curie-Weiss paramagnetic behavior above T_c. Similar phenomena are also observed in Si-doped Gd_4Co_3 with an increased T_c (213 K against 208 K in Gd_4Co_3) [33].

Compared with Gd, the 4*f* band of Gd_6FeBi_2 has a lower energy state (more below the E_F) and shows a clear splitting feature as a results of the hybridization and crystal-field effect (Fig. 6b), suggestive of the higher structural stability. Although it does not produce extra moment, the split peak shifting towards low energy and spin–spin interactions should make it stronger against the vibronic coupling and thus also contribute to an elevated T_c. Such splitting of majority bands seems to be a common feature of electronic structures in the Gd-NME alloys with a high T_c, such as Gd_5Si_4, Gd_4Bi_3 and the present compound [11,17,34]. It is also suggested by the observation that the temperature shift of the vibronic peak was proportional to the splitting of ground level in La-CaMnO perovskite manganites [35]. However, the splitting also implies a wider temperature region of the magnetic transition or a small slope of moment against temperature, leading to small magnetic entropy change as confirmed by experiments on these alloys [34,36–38].

4.3. Crystal-field effects

According to above discussion, the crystal-field effect related to the Gd-Fe hybridization also plays an important role for the high T_c, and thus a brief analysis is needed. The local atomic environments (AEs) around two kinds of Gd atoms in Gd_6FeBi_2 can be representatively depicted as Gd-centered polyhedra, as shown in Fig. 7a and 7b. It is clear that Gd1 at 3 *g* site has an octahedral symmetry marked as O_h, while Gd2 at 3*f* site shows a C_{4v} symmetry in the form of square pyramid. For the O_h symmetry, the sevenfold orbitally degenerate F item of the free Gd atom with one *f* electron in each orbital is split by the octahedral crystal field into three terms as depicted in Fig. 7c: one is nondegenerate (A_{2u}) and two are threefold degenerate (T_{1u} and T_{2u} respectively) [39,40]. The splitting suggests DOS spectra of two main peaks of high energy levels plus a narrow peak of low energy levels. For the C_{4v} symmetry, the F item is split into five terms (three nondegenerate items A_1, B_1, B_2 and two twofold degenerate items E_1 and E_2) by the ligand field of square prism, as shown in Fig. 7d [38]. Generally, the energy gap of the splitting $F \rightarrow A_1 + B_1 + B_2 + E_1 + E_2$ is small, thus one or two broadening 4*f* peak instead of five peaks was expected. In the splitting $F \rightarrow A_{2u} + T_{1u} + T_{2u}$, the energy gaps

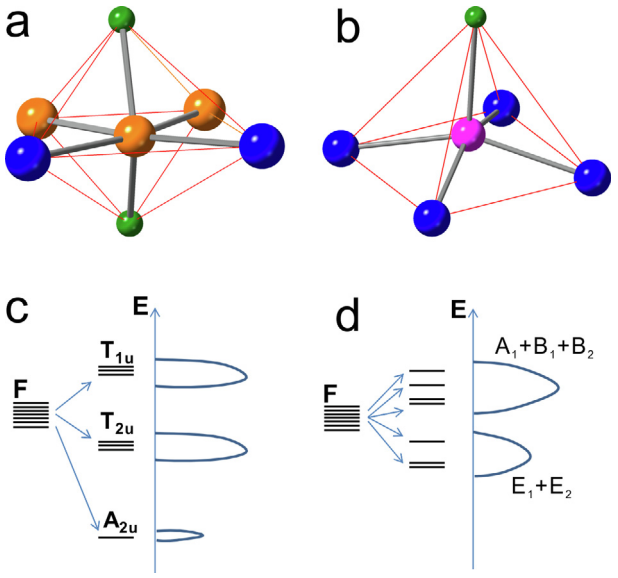

Fig. 7. Atomic environments of Gd atoms in Gd_6FeBi_2: (a) Gd1 atom and (b) Gd2 atom, and schematic ilustration on corresponding crystal-field spliting of energy bands for Gd1 (c) and Gd2 (d).

between T items and F is small compared with that between A and F, and seems similar to that in the splitting of C_{4v} symmetry. Thus a broadening 4*f* peak including T, B, E and A_1 items is expected, while the A_{2u} can be also enclosed or form a split peak. If A_{2u} formed a split peak, the ratio of the small peak to the main peak should be around 1:13 in intensity. The inference is well supported by the observation of a shoulder in the broad Gd 4*f* XPS peak (Fig. 6b). It should be noted that the energy gap of band splitting is highly dependent on the strength of crystal fields and shortly expressed as [38]

$$\Delta = 5/3eqF(R) \quad (17)$$

where *e* is electronic charge, *q* atomic effective charge, *R* is interatomic distance and *F* is a function of *R*. Thus the isostructural compounds can show different electronic structure, e.g. larger splitting energy which can even induce the filling of minor bands, or no observed splitting peak which corresponds for a relatively lower curie temperature. In the viewpoint here, the low T_c in the isostructural Gd_6CoTe_2 can be well understood [31]. In turn, the energy gap of the splitting also is an indicator characterizing the stability of the crystal structure.

5. Conclusions

In conclusion, the critical behaviors of Gd_6FeBi_2 at T_c are investigated comprehensively by isothermal magnetization, and estimated critical exponents are more close to the values predicted by the mean-field model. The analyses based on its crystal and electronic structure show that the Gd-Fe exchange interaction is much weaker than Fe-Fe exchange interaction and thus its influence on the critical behavior is limited, which is likely a typical feature for *RE-TM* alloys without *TM-TM* exchange interactions. Due to the strong Gd-Fe hybridization, the influence of vibronic couplings on the Gd-Fe short-range exchange interaction is diminished, accounting for the high T_c. On the other hand, the crystal-field effect results in the broadening or splitting of *f*-electron bands, which provides another important insight for the elevated T_c in Gd-NME compounds, and remarkably different magnetic behaviors among isostructural compounds.

Acknowledgements

We thank Dr. Z.G. Zheng in South China University of Technology for kind discussions on critical behaviors. The work was supported by National Key R&D Program of China [Grant No. 2016YFE0204200] and also partially supported by a grant from the Research Grants Council of Hong Kong SAR [(RGC Project No.) CityU 11253716].

References

[1] F. Meng, C. Magliocchi, T. Hughbanks, Synthesis, structure and bonding of Gd_6MTe_2 (M = Co, Ni), Er_6RuTe_2, J. Alloys Compd. 358 (2003) 98–103, https://doi.org/10.1016/S0925-8388(03)00456-0.
[2] A.V. Morozkin, New Zr_6CoAs_2-type R_6FeSb_2 (R = Sc, Y, Lu, Dy, Ho, Tm) and Ho_6FeBi_2 compounds, J. Alloys Compd. 353 (2003) L16–L18, https://doi.org/10.1016/S0925-8388(02)01322-1.
[3] L. Zeng, H. Zhao, The 773 K isothermal section of the Ho–Fe–Sb ternary system, J. Alloys Compd. 366 (2004) 201–204, https://doi.org/10.1016/j.jallcom.2003.07.003.
[4] A.V. Morozkin, R. Nirmala, S.K. Malik, Structural and magnetic properties of Fe_2P-type R_6TX_2 compounds (R = Zr, Dy, Ho, Er, T = Mn, Fe Co, Cu, Ru, Rh, X = Sb, Bi, Te), Intermetallics 19 (2011) 1250–1264, https://doi.org/10.1016/j.intermet.2011.04.002.
[5] A.V. Morozkin, New Zr_6CoAs_2-type R_6FeBi_2 (R = Y, Lu, Gd–Dy, Er, Tm) compounds, J. Alloys Compd. 358 (2003) L9–L10, https://doi.org/10.1016/S0925-8388(03)00134-8.
[6] A.V. Morozkin, Magnetic structures of Zr_6CoAs_2-type Ho_6FeSb_2, Ho_6CoBi_2, Ho_6FeBi_2 and Ho_6MnBi_2 compounds, J. Alloys Compd. 395 (2005) 7–16, https://doi.org/10.1016/j.jallcom.2004.11.022.
[7] A.V. Morozkin, V.N. Nikiforov, B. Malaman, Magnetic structure of the Zr_6CoAs_2-type Tb_6FeBi_2 compound, J. Alloys Compd. 393 (2005) L6–L9, https://doi.org/10.1016/j.jallcom.2004.08.103.
[8] G. Cai, J. Zhang, W. He, P. Qin, L. Zeng, Crystal structure and magnetic properties of Tb_6FeSb_2, J. Alloys Compd. 421 (2006) 42–44, https://doi.org/10.1016/j.jallcom.2005.11.020.
[9] W. He, J. Zhang, L. Zeng, P. Qin, G. Cai, Thermomagnetic properties near transitions of Tb_6FeX_2 (X = Sb, Bi), J. Alloys Compd. 443 (2007) 15–19, https://doi.org/10.1016/j.jallcom.2006.10.005.
[10] F. Wang, J. Zhang, F. Yuan, Y. Cao, C. Gao, Y. Hao, J. Shen, J. Sun, B. Shen, Magnetic properties and magnetocaloric effect in $Ho_{6-x}Er_xMnBi_2$ compounds, J. Appl. Phys. 107 (2010) 09A918, https://doi.org/10.1063/1.3359812.
[11] J. Zhang, G. Shan, Z. Zheng, C.H. Shek, Structure and magnetic behaviors of Gd_6FeBi_2 compound, Intermetallics 68 (2016) 51–56, https://doi.org/10.1016/j.intermet.2015.07.013.
[12] A.V. Morozkin, V.K. Genchel, A.V. Knotko, V.O. Yapaskurt, J. Yao, S. Quezado, S.K. Malik, Structural and magnetic properties of Fe2P-type R6TTe2 compounds (R = Tb, Dy, Ho, Er, T = Fe Co, Ru): Magnetic properties and specific features of magnetic entropy change, J. Solid State Chem. 258 (2018) 201–211, https://doi.org/10.1016/j.jssc.2017.10.023.
[13] J. Szade, M. Neumann, Electronic structure investigation of Gd intermetallics, J. Phys.: Condens. Matter 11 (1999) 3887–3896, https://doi.org/10.1088/0953-8984/11/19/308.
[14] J. Szade, M. Drzyzga, Magnetism and electronic structure of Gd_5Bi_3 and Gd_4Bi_3, J. Alloys Compd. 299 (2000) 72–78, https://doi.org/10.1016/S0925-8388(99)00799-9.
[15] T. Nilges, Understanding of magnetic ordering in Gd-rich compounds, Acta Cryst. C 75 (2019) 609, https://doi.org/10.1107/S2053229619007149.
[16] J.O. Dimmock, A.J. Freeman, Band structure and magnetism of gadolinium metal, Phys. Rev. Lett. 13 (1964) 750–752, https://doi.org/10.1103/PhysRevLett. 13.750.
[17] X.B. Liu, Z. Altounian, Exchange interaction in Gd_4Bi_3 and Gd from First-Principles calculations, IEEE Trans. Mag. 45 (2009) 3989–3992, https://doi.org/10.1109/TMAG.2009.2023063.
[18] J. Zhang, Y.M. Kang, G. Shan, S. Bobev, Structural analysis of Gd_6FeBi_2 from single-crystal X-ray diffraction methods and electronic structure calculations, Acta Cryst. C 75 (2019) 562–567, https://doi.org/10.1107/S2053229619004868.
[19] S.N. Kaul, S. Srinath, Gadolinium: A helical antiferromagnet or a collinear ferromagnet, Phys. Rev. B 62 (2000) 1114–1117, https://doi.org/10.1103/PhysRevB.62.1114.
[20] H.E. Stanley, Introduction to Phase Transtions and Critical Phenomena, Oxford University Press, London, 1971.
[21] B.J. Beaudry, A.H. Daane, The Sc-Gd system, J. Less-Common Met. 6 (1964) 322–325, https://doi.org/10.1016/0022-5088(64)90129-8.
[22] L.P. Levy, Magnetism and Superconductivity, Springer-Verlag, Berlin Heidelberg, 2000.
[23] A. Arrott, Criterion for ferromagnetism from observations of magnetic isotherms, Phys. Rev. 108 (1957) 1394–1396, https://doi.org/10.1103/PhysRev.108.1394.
[24] B.K. Banerjee, On a generalised approach to first and second order magnetic transitions, Phys. Lett. 12 (1964) 16–17, https://doi.org/10.1016/0031-9163(64)91158-8.
[25] A. Arrott, J.E. Noakes, Approximate equation of state for nickel near its critical temperature, Phys. Rev. Lett. 19 (1967) 786–789, https://doi.org/10.1103/PhysRevLett.19.786.
[26] S.N. Kaul, Static critical phenomena in ferromagnets with quenched disorder, J. Magn. Magn. Mater. 53 (1985) 5–53, https://doi.org/10.1016/0304-8853(85)90128-3.
[27] A.K. Pramanik, A. Banerjee, Critical behavior at paramagnetic to ferromagnetic phase transition in $Pr_{0.5}Sr_{0.5}MnO_3$: A bulk magnetization study, Phys. Rev. B 79 (2009) 214426, , https://doi.org/10.1103/PhysRevB.79.214426.

[28] J.S. Kouvel, M.E. Fisher, Detailed magnetic behavior of nickel near its Curie point, Phys. Rev. 136 (1964) A1626–A1632, https://doi.org/10.1103/PhysRev.136.A1626.
[29] D. Hohnke, E. Parthé, Rare-earth bismuthides with D88 and Hf_5Sn_3Cu-type structures, J. Less-Common Met. 17 (1969) 291–296, https://doi.org/10.1016/0022-5088(69)90146-5.
[30] L.P. Kadanoff, W. GÖTze, D. Hamblen, R. Hecht, E.A.S. Lewis, V.V. Palciauskas, M. Rayl, J. Swift, D. Aspnes, J. Kane, Static phenomena near critical points: Theory and Experiment, Rev. Mod. Phys. 39 (1967) 395–431, https://doi.org/10.1103/RevModPhys.39.395.
[31] A.V. Morozkin, Y. Mozharivskyj, V. Svitlyk, R. Nirmala, O. Isnard, P. Manfrinetti, A. Provino, C. Ritter, Magnetic properties of Fe_2P-type R_6CoTe_2 compounds (R = Gd–Er), J. Solid State Chem. 183 (2010) 1314–1325, https://doi.org/10.1016/j.jssc.2010.04.002.
[32] S. Legvold, Rare Earth Metals and Alloys, in: E.P. Wohlfarth (Ed.), Handbook of Magentic Materials, North-Holland Publishing Company, North Holland, 1980, pp. 183–296.
[33] Z.G. Zheng, X.C. Zhong, Z.W. Liu, D.C. Zeng, V. Franco, J.L. Zhang, Magnetocaloric effect and critical behavior of amorphous $(Gd_4Co_3)_{1-x}Si_x$ alloys, J. Magn. Magn. Mater. 343 (2013) 184–188, https://doi.org/10.1016/j.jmmm.2013.04.087.
[34] Y.I. Spichkin, V.K. Pecharsky, K.A. Gschneidner, Preparation, crystal structure, magnetic and magnetothermal properties of $(Gd_xR_{5-x})Si_4$, where R = Pr and Tb, alloys, J. Appl. Phys. 89 (2001) 1738–1745, https://doi.org/10.1063/1.1335821.
[35] V.A. Voloshin, A.A. Gusev, I.A. Danilenko, L.I. Medvedeva, A.D. Prokhorov, S.I. Khartsev, Interplay of structure, magnetism and resistivity of $La_{0.5}Ca_{0.54}MnO_{3+x}$, Phys. Lett. A 271 (2000) 121–127, https://doi.org/10.1016/S0375-9601(00)00326-1.
[36] S.Y. Dan'kov, A.M. Tishin, V.K. Pecharsky, K.A. Gschneidner, Magnetic phase transitions and the magnetothermal properties of gadolinium, Phys. Rev. B 57 (1998) 3478–3490, https://doi.org/10.1103/PhysRevB.57.3478.
[37] X.J. Niu, K.A. Gschneidner, A.O. Pecharsky, V.K. Pecharsky, Crystallography, magnetic properties and magnetocaloric effect in $Gd_4(Bi_xSb_{1-x})_3$ alloys, J. Magn. Magn. Mater. 234 (2001) 193–206, https://doi.org/10.1016/S0304-8853(01)00391-2.
[38] J. Zhang, Z. Zheng, G. Shan, S. Bobev, C.H. Shek, Abnormal thermal expansion, multiple transitions, magnetocaloric effect, and electronic structure of $Gd_6Co_{4.85}$, J. Appl. Phys. 118 (2015) 133903, https://doi.org/10.1063/1.4931982.
[39] I.B. Bersuker, Electronic Structure and Peoperties of Transition Metal Compounds: Introduction to the Theory, second ed., John Wiley & Sons Inc, New Jersey, 2010.
[40] G.C. Shan, H.B. Gao, New topological semimetal candidate of nonsymmorphic $PdSb_2$ with unique six-fold degenerate point, Front. Phys. 14 (2019) 43201, https://doi.org/10.1007/s11467-019-0909-0.